ADVANCED MATERIALS
www.advmat.de

Covalent Organic Frameworks as a Decorating Platform for Utilization and Affinity Enhancement of Chelating Sites for Radionuclide Sequestration

*Qi Sun, Briana Aguila, Lyndsey D. Earl, Carter W. Abney, Lukasz Wojtas, Praveen K. Thallapally, and Shengqian Ma**

The potential consequences of nuclear events and the complexity of nuclear waste management motivate the development of selective solid-phase sorbents to provide enhanced protection. Herein, it is shown that 2D covalent organic frameworks (COFs) with unique structures possess all the traits to be well suited as a platform for the deployment of highly efficient sorbents such that they exhibit remarkable performance, as demonstrated by uranium capture. The chelating groups laced on the open 1D channels exhibit exceptional accessibility, allowing significantly higher utilization efficiency. In addition, the 2D extended polygons packed closely in an eclipsed fashion bring chelating groups in adjacent layers parallel to each other, which may facilitate their cooperation, thereby leading to high affinity toward specific ions. As a result, the amidoxime-functionalized COFs far outperform their corresponding amorphous analogs in terms of adsorption capacities, kinetics, and affinities. Specifically, COF-TpAb-AO is able to reduce various uranium contaminated water samples from 1 ppm to less than 0.1 ppb within several minutes, well below the drinking water limit (30 ppb), as well as mine uranium from spiked seawater with an exceptionally high uptake capacity of 127 mg g^{-1}. These results delineate important synthetic advances toward the implementation of COFs in environmental remediation.

Nuclear energy remains at the forefront of low carbon energy sources in an age when climate change has become a serious threat to humanity and at a time when we are in need of alternative energies to replace fossil fuels.[1] The irreplaceable role of the radionuclides is contrasted with their extreme toxicity, raising serious concerns about the hazardous impact of radioactive and toxic waste and thereby motivating the development of new technologies to provide enhanced protection.[2] To efficiently remove and recover radionuclides, it necessitates advanced sorbent materials with not only high binding affinity and selectivity but also rapid kinetics and large capacity.[3] Slow adsorption kinetics and low adsorption capacity significantly diminish the practical utility for the traditional porous materials such as clays, activated carbons, and zeolites.[4] Amorphous porous organic polymers (POP) are potential candidates[5] but their performance is often compromised by buried chelating sites stemmed from the small and irregular pores. In addition, their poorly defined structures complicate characterization and rational improvement. Metal–organic frameworks (MOFs) have been developed for nuclear waste removal based on their crystallinity and amenability to design, but stable performance under a wide range of conditions, such as pH values, remains a challenge.[6] Moreover, adsorbent capacities suffer due to the comparatively large weight fraction attributable to metals comprising the MOF secondary building units. Therefore, porous materials formed solely of light elements that meet the requirements of capacity and stability together with a deliberate and precise preparation are highly desirable.

Covalent organic frameworks (COFs) are an advanced class of porous crystalline materials that enable the specific inclusion of various functionalized units into highly ordered periodic arrays.[7] Their modular structure and extraordinarily broad chemical and reticular/topological variety can be translated into property tunability.[8] This in turn has been underpinned by a broad interest in their investigation as materials for a myriad of applications,[9] most prominent of which are gas separation and storage,[10] catalysis,[11] and optoelectronics.[12] We envision that COFs could offer an attractive alternative platform for mitigating environmental problems caused by the natural and anthropogenic contaminants associated with nuclear energy, in particular, 2D COFs due to their unique structures. The layered

Dr. Q. Sun, B. Aguila, Dr. L. Wojtas, Prof. S. Ma
Department of Chemistry
University of South Florida
4202 E. Fowler Avenue, Tampa, FL 33620, USA
E-mail: sqma@usf.edu
Dr. L. D. Earl, Dr. C. W. Abney
Chemical Sciences Division
Oak Ridge National Laboratory
P.O. Box 2008, Oak Ridge, TN 37831, USA
Prof. P. K. Thallapally
Physical and Computational Science Directorate
Pacific Northwest National Laboratory
Richland, WA 99352, USA
The ORCID identification number(s) for the author(s) of this article can be found under https://doi.org/10.1002/adma.201705479.

DOI: 10.1002/adma.201705479

sheets of these COFs typically adopt nearly eclipsed stacked structures, providing continuous nanometer-scale channels normal to the stacking direction, which provides a path for ions to the chelating groups that comprise the walls. Furthermore, the periodic arrays of aligned chelating groups in 2D COFs are expected to facilitate their cooperation in metal binding. Moreover, the crystallinity of these materials is beneficial in studying the relationship between structure and function. In this sense, we reason that incorporation of a specific ligand into 2D COF walls may provide a solution for the aforementioned challenges, as encountered by other adsorbent materials, and a better system may be developed by integrating the intrinsic advantage of the chelating groups in selectivity and affinity with that of COFs in kinetics and capacity.

Considering the mobility, radioactivity, and high toxicity of uranium, together with its indispensable role in nuclear energy,[13] uranium sequestration was thus chosen as a proof-of-concept study to demonstrate the potential applications of COFs in waste management and nuclear source enrichment to safeguard energy development. To impart COFs with a specific functionality as uranium capturers, amidoxime is the chelating group of choice, given that it has been proven to be the state-of-the-art moiety for uranium mitigation.[14] Therefore, in this contribution, the amidoxime contained moieties were incorporated into 2D COFs linked by irreversible β-ketoenamines to confer outstanding chemical and hydrolytic stability.[15] It is shown that the resultant adsorbents are able to extract uranium from a variety of contaminated waters, indicating the feasibility of COF materials for uranium removal. The performance is further engineered by the reticular design of COFs without altering the underlying topology and the larger open channels can increase the adsorption rate by facilitating mass diffusion. In particular, emphasis is placed on the considerable superiority of the highly ordered 1D pore channel for the design of highly efficient adsorbent materials. We demonstrate this by synthesizing the amorphous POP analog and comparing the POP- and COF-based adsorbent performance. The COF-based adsorbents displayed superior performance in adsorption of uranium as compared to the amorphous POPs in terms of uptake capacities, kinetics, and binding affinities. Due to the similarity in amidoxime-binding site content, we can conclude that the ordered pore structure and relatively high surface area of the COF facilitate uranium uptake compared to the amorphous POP. This work thereby puts forth a promising design strategy in optimizing the performance of adsorbents for environmental remediation.

A two-step synthesis was employed due to the incompatibility of the amidoxime group during COF synthesis as it is prone to react with the building units and, therefore, is likely to inhibit the COF formation. Given that amidoxime groups are readily formed through the reaction of hydroxylamine with cyano groups, a nitrile-functionalized COF was first obtained by condensing 2,5-diaminobenzonitrile (Db) with triformylphloroglucinol (Tp) under solvothermal conditions to yield COF-TpDb (**Figure 1**). The resultant COF was then amidoximated by treatment with hydroxylamine in methanol to afford the amidoxime-functionalized COF material (COF-TpDb-AO). The chemical composition and structure of COF-TpDb were determined by Fourier transform infrared (FT-IR) and solid-state ^{13}C NMR spectroscopy. The disappearance of the characteristic primary N—H stretching bands (3300–3400 cm^{-1}) of the parent amines and the C=O stretching frequency around 1660 cm^{-1} for aldehydes in the FT-IR spectrum of COF-TpDb indicates the complete consumption of the starting materials. In addition, the absence of the C=N stretching peaks at around 1634 cm^{-1} and the emergence of a new C—N stretch at 1230 cm^{-1} verify the transformation of the enol to keto tautomer (Figure S1, Supporting Information).[16] Furthermore, the peak observed at 2213 cm^{-1}, which is ascribed to the CN stretching band, indicates the existence of cyano groups in COF-TpDb (**Figure 2**f). The amount of cyano groups in COF-TpDb was determined to be 4.2 mmol g^{-1} by CHN analysis, which is consistent with the theoretical result. Solid-state ^{13}C NMR spectrum of COF-TpDb provides a separate line of evidence for the existence of the keto tautomer and cyano functionality, supported by the presence of the peak at about 183 and 95 ppm, which are attributed to the keto (C=O) and CN group, respectively (Figure 2g).

To analyze the structure of COF-TpDb, powder X-ray diffraction (PXRD) experiments were conducted (Figure 2a). In the experimental PXRD profile of COF-TpDb, a strong peak at 4.8° together with some relatively weaker peaks at 8.1°, 12.3°, 15.8°, and ≈26.9° was observed, which were assigned to (100), (110), (210), (220), and (001) diffractions (Figure 2a). To elucidate the lattice packing, theoretical simulations using Materials Studio were performed by constructing structural models (Table S1, Supporting Information). Full profile pattern matching (Pawley) refinements were carried out on the experimental PXRD, and the refined PXRD pattern is in good agreement with the experimental results, as evidenced by the negligible difference (Figure S2, Supporting Information). The experimental data matched well with the simulated PXRD patterns of the proposed model in an eclipsed orientation (AA stacking, Figure 2b). In contrast, staggered orientations (AB stacking, Figure 2c) show significant deviations from the observed PXRD patterns. These results show that COF-TpDb has 1D channels, with a diameter of 15.8 Å, stacking along the *c*-axis with an interlayer distance of 3.4 Å. To investigate the details of the pore characteristics of COF-TpDb, N_2 sorption measurements at 77 K were performed. The Brunauer–Emmett–Teller (BET) surface area of COF-TpDb was evaluated to be 1164 m^2 g^{-1} (Figure 2d) with a pore size distribution centered at 15.4 Å (Figure S3, Supporting Information) calculated by using the nonlocal density functional theory (DFT) method, which is in good agreement with the theoretical value.

With a porous and crystalline nitrile-functionalized framework available, we proceeded to convert the cyano groups to amidoxime by reacting with hydroxylamine. The PXRD pattern of the obtained material exhibits a diffraction pattern comparable to the one of COF-TpDb with an intense reflection at 4.8° (Figure 2a). N_2 sorption measurements were conducted to verify pore accessibility after the postsynthetic conversion, affording isotherms similar to those of COF-TpDb. The BET surface area was calculated to be 826 m^2 g^{-1}, indicating the retention of porosity after the amidoximation process (Figure 2e). Scanning electron microscope (SEM) images of COF-TpDb-AO show a rough surface composed of thin rods, which is similar to the observed morphology of COF-TpDb, suggesting the structural integrity during the chemical transformation process (Figure S4,

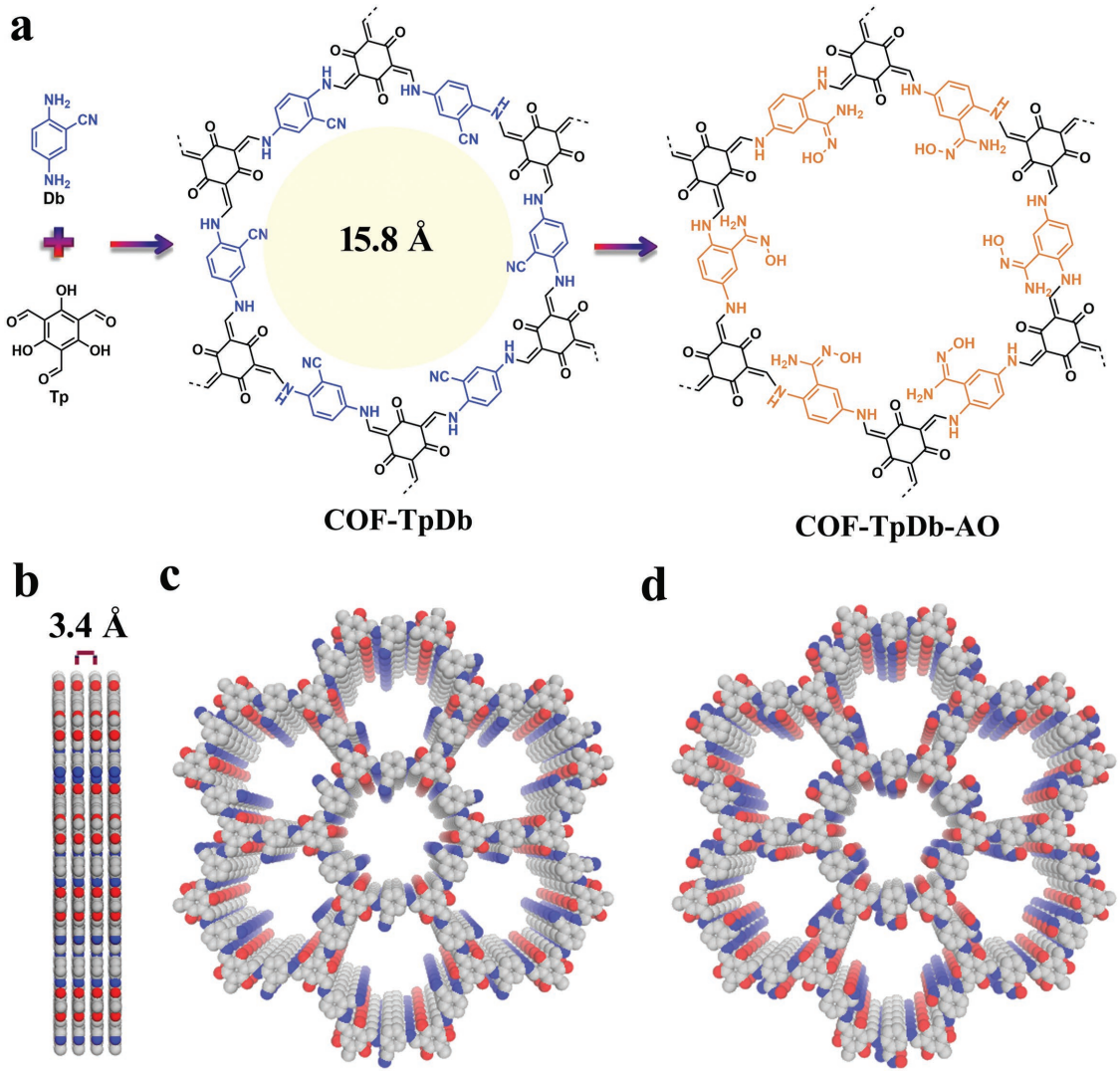

Figure 1. a) Synthetic scheme of COF-TpDb through the condensation of Tp (black) and Db (blue) and corresponding chemical transformation from the cyano to amidoxime group, yielding COF-TpDb-AO. b,c) Graphic view of the eclipsed AA stacking structure of COF-TpDb (blue, N; gray, C; red, O; hydrogen is omitted for clarity). d) Graphic view of COF-TpDb-AO (blue, N; gray, C; red, O; hydrogen is omitted for clarity).

Supporting Information). To study the postsynthetic conversion and the amidoxime formation, FT-IR and solid-state ^{13}C NMR spectroscopy were carried out. Successful amidoximation was indicated by the disappearance of the C≡N stretch (2213 cm^{-1}) and the appearance of C=N (1646 cm^{-1}) and N—O (924 cm^{-1}), characteristic peaks of the amidoxime group in the FT-IR spectrum of COF-TpDb-AO (Figure 2f). Furthermore, solid-state ^{13}C NMR analysis confirmed this efficient transformation, as indicated by the disappearance of the peak at 95 ppm that is related to CN groups together with the concomitant emergence of a peak at 169 ppm that is ascribed to open-chain amidoxime groups (Figure 2g).[17] Moreover, the stability of COF-TpDb-AO is also very impressive, as demonstrated by the fact that it could retain the crystalline structure within a wide pH range (3 M NaOH or 3 M HCl) and high ionic strength (saturated NaCl). Furthermore, negligible change in the IR spectra was observed after exposure to the above conditions, which is vitally important for practical applications (Figures S5 and S6, Supporting Information).

Given the hydrolytic stability, robust 2D architecture, and channelized alignment of the chelating groups, the ability of COF-TpDb-AO to trap uranium was investigated. Experiments were initially performed to estimate the uranium uptake capacity from aqueous solutions. To determine whether the long-range order pore structures of the adsorbents influence the sequestration performance, head-to-head comparisons were made with the amorphous analog, POP-TpDb-AO (BET: 466 $m^2\ g^{-1}$; Figures S7 and S8, Supporting Information). This material was synthesized by condensation of triformylphloroglucinol with 2,5-diaminobenzonitrile and then amidoximated as described above. Elemental analysis and FT-IR spectroscopy were performed to determine the content of amidoxime species in the adsorbent material (see the "Experimental Section" and Figure S9 in the Supporting Information). Both the COF-based adsorbent and its amorphous POP analog showed very similar N element contents in conjunction with comparable FT-IR spectra before and after the amidoximation process, indicative

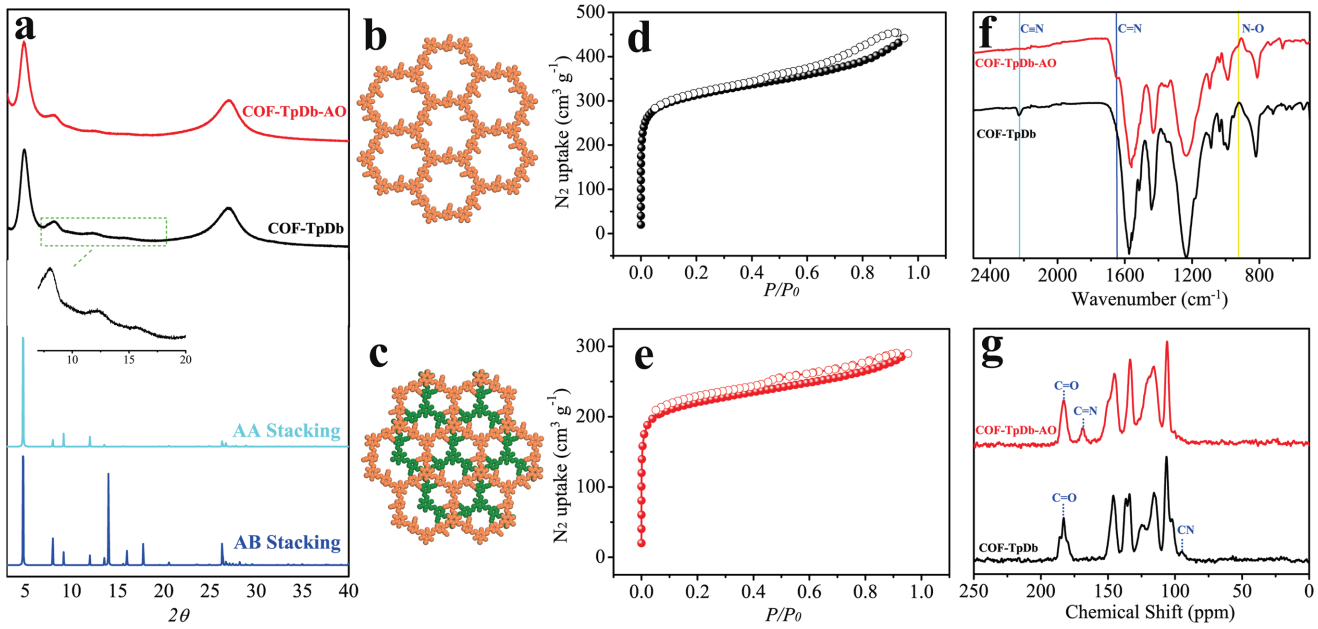

Figure 2. a) PXRD profiles. b) AA stacking mode of COF-TpDb. c) AB stacking mode of COF-TpDb. d,e) Nitrogen-sorption isotherm curves measured at 77 K for COF-TpDb and COF-TpDb-AO, respectively. f) IR spectra. g) Solid-state ^{13}C NMR spectra.

of a similar number of amidoxime functionalities (Figure S10, Supporting Information).

The amounts of uranium species enriched by these materials as a function of uranium concentration in supernatant at the equilibrium state were determined by varying the initial concentrations from 23.1 to 265.2 ppm at a pH value around 6 with an adsorbent-to-solution ratio of 0.45 mg mL^{-1}. To guarantee the adsorptions reached equilibrium, an overnight stirring step was used. As shown in **Figure 3**a, a continuous increase of uranium sorption with augmentation of the initial uranium concentrations was observed. All the adsorption isotherms were found to follow a Langmuir model with correlation coefficients higher than 0.98 (Figure S11, Supporting Information). The COF-based adsorbent showed superior performance in adsorption of uranium in terms of saturation adsorption capacity as compared to the amorphous porous polymer analog, suggesting a role of the material's architecture. Specifically, in the initial uranium concentration range of 23.1–265.2 ppm, the saturation adsorption capacities were determined to be 408 and 355 mg g^{-1}, for COF-TpDb-AO and POP-TpDb-AO, respectively. The synergistic effects of densely populated yet highly accessible chelating groups on the ordered 1D channels place COF-TpDb-AO among the best amidoxime-functionalized sorbent materials (Table S3, Supporting Information). Moreover, the shape of the isotherms for these adsorbents is somewhat varied, especially at low C_e concentrations. The COF-based adsorbent exhibits a much steeper adsorption profile for uranyl ions (Figure 3b), suggesting that it possesses higher affinities toward uranyl ions in comparison with the corresponding amorphous porous polymer.

To further underscore the advantage of using COFs as a platform for the deployment of efficient adsorbent materials, adsorption kinetics between the COF-based sorbent and amorphous counterpart were compared, considering that this parameter largely defines the adequate flow rate for decontamination of polluted water and the subsequent efficiency of the process.

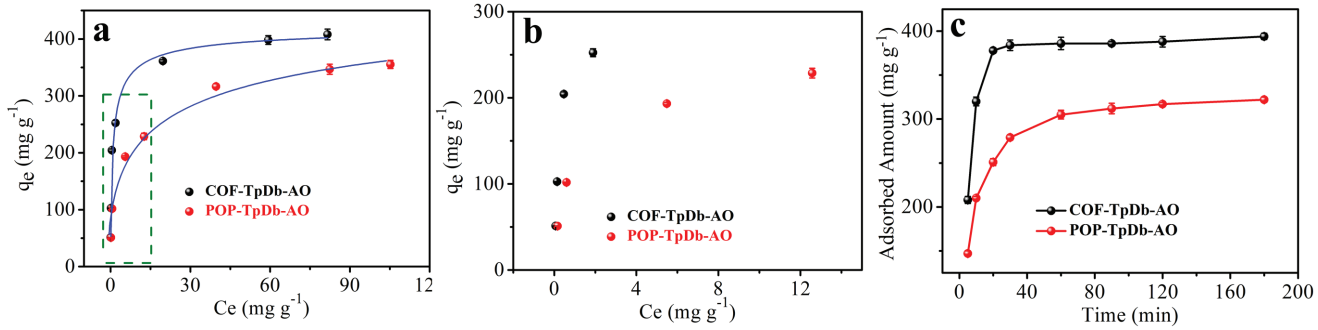

Figure 3. a) Uranium sorption isotherms for COF- and POP-based sorbents. The lines are fit with the Langmuir model; all the fits have R^2 values higher than 0.98. b) Enlarged section of green rectangle in panel (a). c) The kinetics of uranium adsorption from aqueous solution with an initial concentration of 9.25 ppm (400 mL), at pH≈6, and adsorbent material (4.5 mg).

The impact of contact time on uranium adsorption was investigated by immersing the adsorbents in the uranium-spiked solution for a period ranging from 5 min to 3 h. As depicted in Figure 3c, in comparison to COF-based adsorbent, the POP analog displayed inferior adsorption kinetics. Under identical conditions, COF-TpDb-AO can reach 81% and 95% of its equilibrium adsorption capacity within 10 and 30 min, respectively. However, it took 90 min for POP-TpDb-AO to accomplish around 95% of its equilibrium adsorption capacity. Both adsorption kinetic processes were well fitted with the pseudo-second-order kinetic model, yielding rate constants of 398.4 and 333.3 g mg^{-1} min^{-1} for COF-TpDb-AO and POP-TpDb-AO, respectively, confirming that the COF-based sorbent exhibits a higher adsorption rate in relation to its amorphous analog (Figure S12, Supporting Information). Notably, in addition to rapid saturation, COF-TpDb-AO also possessed a higher capacity, yielding an equilibrium value of 394 mg g^{-1}, while its amorphous analog only achieved 322 mg g^{-1}, the average of multibatch experiments (Figure S13, Supporting Information). Taking into account that the COF- and POP-based sorbents have the same chemical compositions, the high uptake capacity and rapid sorption should be ascribed to their difference in pore architecture. In COF-based sorbents, the amidoxime groups that are uncovered on the regular and ordered pore channels are highly accessible, thereby facilitating the chelating groups to trap uranyl ions. In contrast, the irregular pore channels in amorphous POPs are discontinuous, making them more susceptible to blockage and therefore greatly compromising their adsorption performance, as shown schematically in **Figure 4**. However, it is to be noted that due to the difference in surface area of COF-TpDb-AO and POP-TpDb-AO (826 vs 466 m^2 g^{-1}), we cannot fully conclude that structural differences in the adsorbent framework are responsible for their discrepancy in adsorption performance. In this context, to rule out the possibility of the improved performance in uranium adsorption of COF-TpDb-AO in relation with POP-TpDb-AO is mainly contributed to their discrepancy in surface area, an amidoxime-functionalized amorphous polymer (PAF-1-CH_2AO, BET = 855 m^2 g^{-1}, amidoxime group content of 1.7 mmol g^{-1}), which was developed by our group, was selected for comparison.[5c] Time-course adsorption measurements revealed that PAF-1-CH_2AO reached 84.4% of its equilibrium capacity after 1 h with an increase to 95.8% after 3 h, much inferior to that of COF-TpDb-AO. In addition, due to the lower functional group density, PAF-1-CH_2AO also afforded inferior adsorption capacity in relation to COF-TpDb-AO (283 vs 408 mg g^{-1}). These results indicate the superiority of COFs as a platform for designing high-performance adsorbents, where a high density yet fully accessible functional groups can be predictably incorporated into ordered pore walls.

Apart from the accessibility of binding sites, the pore architecture is assumed to result in different orientations and distribution of the functionalities, which may affect their cooperation with each other, thereby leading to different binding strengths toward the guests. To evaluate the affinity of these materials to uranyl ions, the distribution coefficient values (K_d) were measured. Under the conditions of 5 ppm uranium at pH≈6.0 with a V/m of 10 000 mL g^{-1}, the K_d values for these samples were calculated and found to equal 3.6×10^8 (0.14 ppb) and 3.3×10^7 (1.51 ppb) for COF-TpDb-AO and POP-TpDb-AO, respectively (number given in parenthesis is the residual uranium concentration), with the COF showing more than an order of magnitude improvement in performance over its amorphous analog. Recent publications leveraged DFT calculations and crystallography to predict an η^2 binding interaction to be most thermodynamically favored between amidoxime and uranyl.[18] In addition, a chelating di(oximate) uranyl complex was also collected where no tautomerization was observed, indicating that neighboring amidoxime groups could bind uranyl ions in a 2:1 ratio.[19] In this context, we reasoned that convergent orientation of the amidoxime groups at adjacent layers of COF materials is believed to facilitate the formation of multidentate binding with uranyl ions, which leads to the observed high affinity.

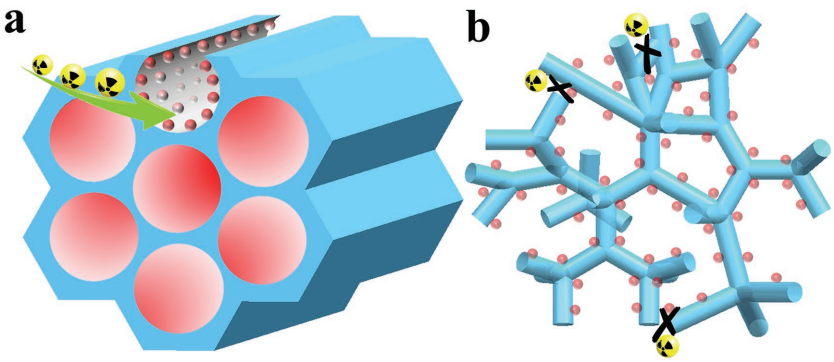

Figure 4. a) Schematic illustration of chelating groups in COF materials. The uniform pore morphology of the COFs leads to the functionalized material with unrestricted access of ions to all of the chelating sites. b) The functionalization of amorphous porous organic polymers, illustrating the blockage of narrow pore channels and bottlenecks. Pore blocking is likely to impede access of metal ions to the functional sites in POPs.

To further illustrate the benefit of COFs as an appealing functionality decorating platform for radionuclide sequestration, another amidoxime-functionalized COF material (COF-TpAab-AO, **Figure 5**; Table S2, Supporting Information) and corresponding amorphous analog (POP-TpAab-AO, BET = 513 m^2 g^{-1}) were prepared for comparison. The detailed characterization of these materials is shown in Figures S14–S25 (Supporting Information). Again, the COF-based sorbent favored superior adsorption performance to that of its amorphous analog in terms of both uranium uptake capacity and removal efficiency (Figures S26–S29, Supporting Information). Specifically, COF-TpAab-AO and POP-TpAab-AO afforded the uranium saturation uptake capacities of 305 and 256 mg g^{-1}, respectively. In addition, COF-TpAab-AO was three times faster than that of POP-TpAab-AO to reach their 95% equilibrium capacities (Figure S26c, Supporting Information). Furthermore, a pronounced improvement of affinity toward uranium was also observed, as demonstrated by a higher K_d value of the COF in relation to that of the POP by a factor of 10 (2.2×10^8 vs 1.8×10^7).

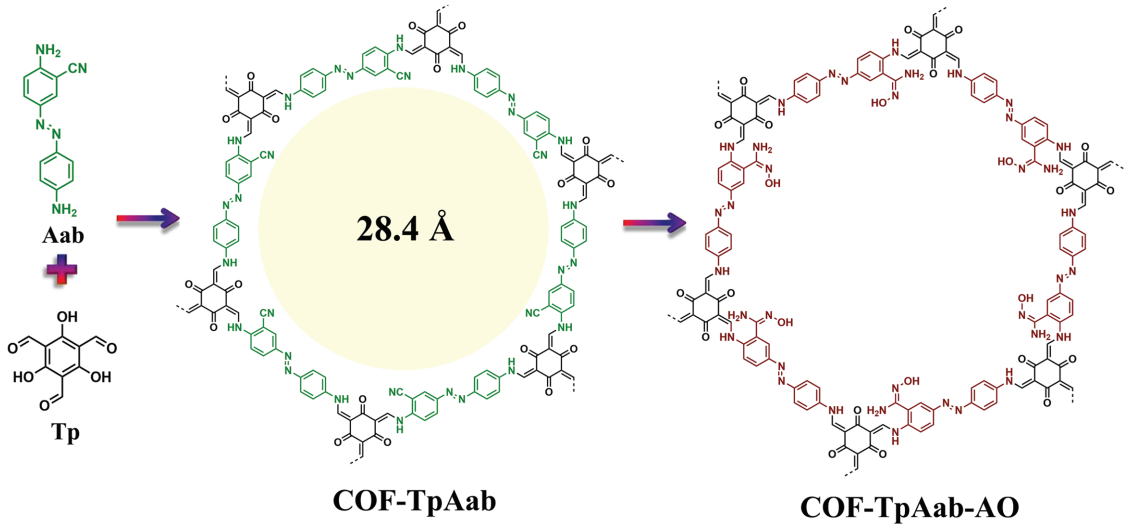

Figure 5. Synthetic scheme of COF-TpAab through the condensation of Tp (black) and Aab (green) and corresponding chemical transformation from the cyano to amidoxime group, yielding COF-TpAab and COF-TpAab-AO, respectively.

It is worth mentioning that a slightly faster uptake of COF-TpAab-AO compared with COF-TpDb-AO, in terms of the rate to reach equilibrium capacity, is observed, which is likely related to pore size (Figure S30, Supporting Information). Diffusion of uranium species within COF-TpAab-AO with a larger pore size is expected to be more rapid than that within COF-TpDb-AO. Nonetheless, the difference is not obvious between the two COF adsorbents, thus suggesting that the chelating groups on both COF walls can be readily accessible. COF-TpDb-AO and COF-TpAab-AO can reach 81% and 87% of their equilibrium adsorption capacity within 10 min, respectively, and both of them can reach over 95% within 30 min. These results thereby highlight that the ordered and regular pore channels of COFs enable the functionalities decorated to be more accessible.

To trace the interaction between the sorbents and uranium species, elemental distribution mapping and X-ray photoelectron spectroscopy (XPS) studies were performed. Uranium species included COF-TpDb-AO and POP-TpDb-AO (U@COF-TpDb-AO and U@POP-TpDb-AO) were chosen as representative samples for these studies. Elemental distribution mapping shows the presence of significant amounts of captured uranium and its homogeneous distribution in the sample (Figures S31 and S32, Supporting Information). XPS spectra exhibited strong U 4f peaks, giving the U $4f_{5/2}$ binding energies at 392.4 and 392.7 eV for U@COF-TpDb-AO and U@POP-TpDb-AO, respectively, which is significantly lower than that of $UO_2(NO_3)_2 \cdot 6H_2O$ (393.4 eV). These results indicate that strong interactions exist between the uranium species and COF-TpDb-AO (Figure S33, Supporting Information). The obvious redshift of the antisymmetric vibration of $[O{=}U{=}O]^{2+}$ in COF-TpDb-AO (933 cm^{-1}; Figure S34, Supporting Information) and POP-TpDb-AO (938 cm^{-1}) in comparison with that in $UO_2(NO_3)_2 \cdot 6H_2O$ (≈960 cm^{-1}) from the IR studies further confirms the XPS results.[20] The slight differences in the binding energy of the uranium species and the antisymmetric vibration of $[O{=}U{=}O]^{2+}$ in COF-TpDb-AO and POP-TpDb-AO suggest that coordination dissimilarities exist between the uranium species and amidoxime groups in these sorbents.

To gain more insight into the coordination environment of uranium in both COF-TpDb-AO and POP-TpDb-AO, we employed X-ray absorption fine structure (XAFS) spectroscopy collected at the U L_{III}-absorption edge (17.166 keV). Fits of the extended XAFS (EXAFS) data for COF-TpDb-AO and POP-TpDb-AO were performed simultaneously and are shown in **Figure 6** and Tables S4–S6 (Supporting Information, and also see for experimental details and analysis). Inspection of the data suggests the U(VI) coordination environment is similar between the two porous frameworks, and reasonable fits are obtained from applying the same uranyl-benzamidoxime η^2 binding motif model to both COF-TpDb-AO and POP-TpDb-AO. Two distinct U—O distances are required within the equatorial coordination plane, consistent with η^2 binding;[18] however, the spectral resolution of the data (≈0.2 Å) precludes definitive assignment of the uranium coordination environment. Nevertheless, the successful simultaneous fitting of the EXAFS data sets with the same structure model, in conjunction with affording refined parameters within experimental uncertainty of each other, demonstrates a common uranium-binding mode.

Investigation of the wavelet transform provides further support for a common uranium-binding environment between both POP and COF materials (Figures 6e,f). In contrast to the commonly used Fourier transform, the wavelet transform provides information regarding the localization of different EXAFS signal components in both *k*- and *R*-spaces simultaneously. This approach affords superior discrimination of EXAFS contributions from different species, as the phase and backscattering amplitude from different elements are emphasized in different regions of *k*-space.[21] As a corollary, multiple scattering paths from light elements, which possess the same half-path length as direct scattering paths from heavier elements, can be readily deconvoluted through simple inspection of the wavelet transform.[22] The similarity between wavelet transforms for POP

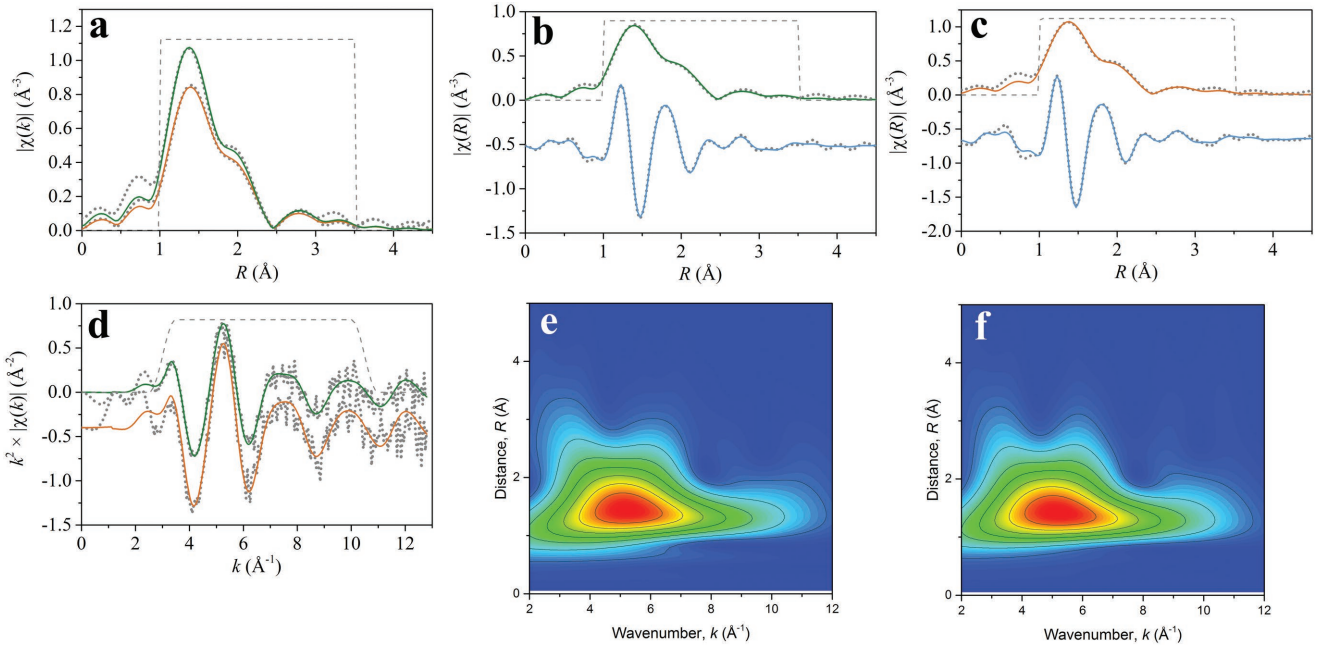

Figure 6. a) Fourier transform of the U L_{III}-edge EXAFS spectra of POP-TpDb-AO (green line) and COF-TpDb-AO (orange line) in *R*-space. b) Fourier transform of the U L_{III}-edge EXAFS spectrum of COF-TpDb-AO in *R*-space. The magnitude of the Fourier transform is fit by a green line; the real component is fit with a blue line. c) Fourier transform of the U L_{III}-edge EXAFS spectrum of POP-TpDb-AO in *R*-space. The magnitude of the Fourier transform is fit by an orange line; the real component is fit with a blue line. d) Accompanying k^2-weighted $\chi(k)$ data and fit for POP and COF (green and orange lines, respectively). e) Wavelet transform analysis of COF-TpDb-AO and f) POP-TpDb-AO, demonstrating the extreme similarity between data sets. In all panels, gray dashes denote the fit window.

and COF systems, despite the increased information afforded through simultaneous inspection of both *k*- and *R*-signal components, suggests identical uranium-binding environments. However, it should be noted that the exact coordination fashion, such as the angle of two amidoxime groups to UO_2^{2+} ions, is not clear due to the resolution limit of the XAFS. Nevertheless, the observed improved performance of the COF-based adsorbents suggests that the well-oriented chelating groups on the COFs are more ready to bind with uranium species in comparison with the randomly populated form in the POPs. This was predicated by the previous computation results that the binding angle of amidoxime groups and uranyl ions affects the overall energy of the resultant complex,[18] with the above IR and XPS results further confirming such differences exist. Thus, we conclude structural differences in the adsorbent framework are responsible for the divergent performance.

The ability to regenerate and recycle the adsorbent for recovery of uranium would afford great advantages to reducing overall cost and facilitate industrial application (see details in the Supporting Information). Significantly, the possibility of reusing regenerated COF-based sorbents is established over several cycles with negligible loss in uranium extraction capacity suggesting adequate chemical and structural stability of the adsorbent materials. For example, COF-TpDb-AO can readily be regenerated by Na_2CO_3 solution and maintain its original adsorption capacity for at least three cycles, affording 394, 387, and 395 mg g^{-1}, respectively. Moreover, the retained crystallinity of COF-TpDb-AO after the uranium adsorption is evident by the PXRD pattern as shown in Figure S35 (Supporting Information). These results thus reveal the exceptional potential of COFs to serve as high-performance radionuclide scavengers.

Encouraged by the results described above, we were then motivated to evaluate its applicability in real water samples including potable water, well water, and river water, in which uranium was intentionally added at a dilute concentration (1000 ppb). A single treatment with COF-based materials reduced the uranium concentrations in these water samples to less than 0.1 ppb, which is two orders of magnitude lower than the U.S. Environmental Protection Agency elemental limits for hazardous wastes and even drinking water standards (30 ppb). In addition to the impressive removal performance, it is outstanding from the viewpoint of kinetic efficiency, reaching equilibrium capacity within 30 min, whereas over 99.7% of uranium species were removed within 5 min with a high V/m ratio of 10 000 mL g^{-1} (**Figure 7**a). These results highlight the vast potential of COF-based adsorbents as promising candidates in accomplishing radionuclide removal from water.

After demonstrating the ability of COF-TpDb-AO to capture uranium with good affinity and selectivity in the aforementioned situations, we examined its performance in seawater samples for the specific application of mining uranium from seawater for nuclear fuel production.[23] This is an ambitious task as seawater is characterized by substantially high ionic strength and a variety of interfering ions. To test the applicability of the adsorbents for the enrichment of uranium from seawater, the tests were performed using seawater samples spiked with 20 ppm uranium. COF-TpDb-AO showed high uptake capacities, giving rise to as high as 127 mg uranium per gram of adsorbent. In addition to this, the kinetics of uranium capture

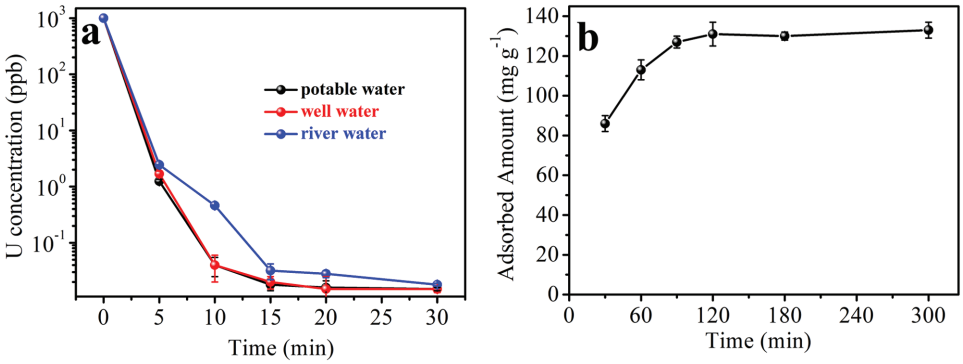

Figure 7. a) The kinetics of uranium removal efficiency of COF-TpDb-AO from various water samples spiked with uranium (1000 ppb) at V/m = 10 000 mL g^{-1}. b) The kinetics of uranium adsorption from seawater spiked with 20 ppm uranium at a V/m = 40 000 mL g^{-1}.

in seawater samples were also found to be very fast and the adsorption equilibrium was reached within 90 min (Figure 7b), encouraging for the potential use of COF-TpDb-AO for the enrichment of uranium from seawater.

In summary, this work has demonstrated, using an example of radionuclide capture, the greatly improved accessibility and affinity of the binding sites toward guest ions in the adsorbents designed from well-defined channels, relative to those prepared from materials with disordered pore networks. The contact area offered by the COF scaffolds maximizes the interaction of the covalently attached chelating groups with uranium species. In addition, the chelating groups aligned in periodic arrays on the walls are proximate with each other, which facilitate their cooperation, thereby leading to high affinities toward uranyl ions. As a result, the adsorbents based on COF materials have shown excellent adsorption performance in comparison with that of amorphous polymers in terms of uptake capacity, kinetics, and removal efficiency in uranium capture. Furthermore, COF-TpDb-AO proves to be feasible for decontamination of the uranium-polluted environmental water samples as well as enrichment of uranium from seawater with great efficiency. Moreover, these materials have been shown to be reusable over several cycles while maintaining good structural and chemical stability, demonstrating the great potential that such porous adsorbents could replace more traditional technologies. Our work thereby highlights new opportunities in using COFs as a novel platform for the deployment of adsorbent materials for environmental remediation by taking advantage of their amenability to design and unique structures.

Supporting Information

Supporting Information is available from the Wiley Online Library or from the author.

Acknowledgements

This work was supported by the DOE Office of Nuclear Energy's Nuclear Energy University Program (Grant No. DE-NE0008281); partial financial support from the US National Science Foundation (CBET-1706025) was also acknowledged. Work by L.D.E. and C.W.A. was supported by the U.S. Department of Energy, Office of Nuclear Energy. This manuscript was authored by UT—Battelle, LLC under Contract No. DE-AC05-00OR22725 with the U.S. Department of Energy. The United States Government retained and the publisher, by accepting the article for publication, acknowledged that the United States Government retains a nonexclusive, paid-up, irrevocable, worldwide license to publish or reproduce the published form of this manuscript, or allow others to do so, for United States Government purposes. The Department of Energy will provide public access to these results of federally sponsored research in accordance with the DOE Public Access Plan (http://energy.gov/downloads/doe-public-access-plan). Use of the Stanford Synchrotron Radiation Lightsource, SLAC National Accelerator Laboratory, was supported by the U.S. Department of Energy, Office of Science, Office of Basic Energy Sciences under Contract No. DE-AC02-76SF00515.

Conflict of Interest

The authors declare no conflict of interest.

Keywords

amidoxime chelating groups, covalent organic frameworks, environmental remediation, radionuclide sequestration, uranium capture

Received: September 21, 2017
Revised: January 26, 2018
Published online: March 27, 2018

[1] a) D. S. Sholl, R. P. Lively, *Nature* **2016**, *532*, 435; b) Y. Lu, *Nat. Chem.* **2014**, *6*, 175; c) Y. Yue, R. T. Mayes, J. Kim, P. F. Fulvio, X.-G. Sun, C. Tsouris, J. Chen, S. Brown, S. Dai, *Angew. Chem., Int. Ed.* **2013**, *52*, 13458; d) C. Liu, P.-C. Hsu, J. Xie, J. Zhao, T. Wu, H. Wang, W. Liu, J. Zhang, S. Chu, Y. Cui, *Nat. Energy* **2017**, *2*, 17007; e) J. Xie, Y. Wang, W. Liu, X. Yin, L. Chen, Y. Zou, J. Diwu, Z. Chai, T. E. Albrecht-Schmitt, C. Liu, S. Wang, *Angew. Chem., Int. Ed.* **2017**, *56*, 7500; f) C. W. Abney, R. T. Mayes, T. Saito, S. Dai, *Chem. Rev.* **2017**, *117*, 13935.

[2] a) D. Banerjee, D. Kim, M. J. Schweiger, A. A. Kruger, P. K. Thallapally, *Chem. Soc. Rev.* **2016**, *45*, 2724; b) A. E. V. Gorden, J. Xu, K. N. Raymond, *Chem. Rev.* **2003**, *103*, 4207; c) D. J. Yang, Z. Feng, H. Y. Zhu, H. W. Liu, X. P. Gao, *Adv. Mater.* **2008**, *20*, 2777; d) K. Buesseler, M. Aoyama, M. Fukasawa, *Environ. Sci. Technol.* **2011**, *45*, 9931; e) E. Macerata, E. Mossini, S. Scaravaggi, M. Mariani, A. Mele, W. Panzeri, N. Boubals, L. Berthon, M.-C. Charbonnel, F. Sansone, A. Arduini, A. Casnati, *J. Am. Chem.*

Soc. **2016**, *138*, 7232; f) S. Wang, E. V. Alekseev, J. Diwu, W. H. Casey, B. L. Phillips, W. Depmeier, T. E. Albrecht-Schmitt, *Angew. Chem., Int. Ed.* **2010**, *49*, 1057; g) L. Xian, G. Tian, C. M. Beavers, S. J. Teat, D. K. Shuh, *Angew. Chem., Int. Ed.* **2016**, *55*, 4671.

[3] a) S. Komarneni, N. Kozai, W. J. Paulus, *Nature* **2001**, *410*, 771; b) G. E. Fryxell, Y. Lin, S. Fiskum, J. C. Birnbaum, H. Wu. *Environ. Sci. Technol.* **2005**, *39*, 1324; c) S. Ma, L. Huang, L. Ma, Y. Shim, S. M. Islam, P. Wang, L.-D. Zhao, S. Wang, G. Sun, X. Yang, M. G. Kanatzidis, *J. Am. Chem. Soc.* **2015**, *13*, 3670; d) L. Ling, W.-x. Zhang, *J. Am. Chem. Soc.* **2015**, *137*, 2788; e) S. J. Tesh, T. B. Scott, *Adv. Mater.* **2014**, *26*, 6056; f) H. Yang, M. Luo, L. Luo, H. Wang, D. Hu, J. Lin, X. Wang, Y. Wang, S. Wang, X. Bu, P. Feng, T. Wu, *Chem. Mater.* **2016**, *28*, 8774; g) C. W. Abeny, K. M. L. Taylor-Pashow, S. R. Russell, Y. Chen, R. Samantaray, J. V. Lockard, W. Lin, *Chem. Mater.* **2014**, *26*, 5231.

[4] a) W. Chouyyok, J. W. Pittman, M. G. Warner, K. M. Nell, D. C. Clubb, G. A. Gill, R. S. Addleman, *Dalton Trans.* **2016**, *45*, 11312; b) A. Mellah, S. Chegrouche, M. Barkat, *J. Colloid Interface Sci.* **2006**, *296*, 434.

[5] a) Y. H. Sihn, J. Byun, H. A. Patel, W. Lee, C. T. Yavuz. *RSC Adv.* **2016**, *6*, 45968; b) N. Sahiner, H. Yu, G. Tan, J. He, V. T. John, D. A. Blake, *ACS Appl. Mater. Interfaces* **2012**, *4*, 163; c) B. Li, Q. Sun, Y. Zhang, C. Abney, B. Aguila, W. Lin, S. Ma, *ACS Appl. Mater. Interfaces* **2017**, *9*, 12511; d) X. Han, M. Xu, S. Yang, J. Qian, D. Hua, *J. Mater. Chem. A* **2017**, *5*, 5123.

[6] a) M. Carboni, C. W. Abney, S. Liu, W. Lin, *Chem. Sci.* **2013**, *4*, 2396; b) W. Yang, Z.-Q. Bai, W.-Q. Shi, L.-Y. Yuan, T. Tian, Z.-F. Chai, H. Wang, Z.-M. Sun, *Chem. Commun.* **2013**, *49*, 10415; c) Z.-Q. Bai, L.-Y. Yuan, L. Zhu, Z.-R. Liu, S.-Q. Chu, L.-R. Zheng, J. Zhang, Z.-F. Chai, W.-Q. Shi, *J. Mater. Chem. A* **2015**, *3*, 525; d) L. Li, W. Ma, S. Shen, H. Huang, Y. Bai, H. Liu, *ACS Appl. Mater. Interfaces* **2016**, *8*, 31032.

[7] a) A. P. Côté, A. I. Benin, N. W. Ockwig, M. O'Keeffe, A. J. Matzger, O. M. Yaghi, *Science* **2005**, *310*, 1166; b) X. Feng, X. Ding, D. Jiang, *Chem. Soc. Rev.* **2012**, *41*, 6010; c) S.-Y. Ding, W. Wang, *Chem. Soc. Rev.* **2013**, *42*, 548; d) Y. Jin, Y. Hu, W. Zhang, *Nat. Rev. Chem.* **2017**, *1*, s41570; e) Z.-F. Pang, S.-Q. Xu, T.-Y. Zhou, R.-R. Liang, T.-G. Zhan, X. Zhao, *J. Am. Chem. Soc.* **2016**, *138*, 4710; f) M. R. Rao, Y. Fang, S. De Feyter, D. F. Perepichka, *J. Am. Chem. Soc.* **2017**, *139*, 2421; g) G. Lin, H. Ding, D. Yuan, B. Wang, C. Wang, *J. Am. Chem. Soc.* **2016**, *138*, 3302; h) R. P. Bisbey, W. R. Dichtel, *ACS Cent. Sci.* **2017**, *3*, 533.

[8] a) A. G. Slater, A. I. Cooper, *Science* **2015**, *348*, aaa8075; b) S. Das, P. Heasman, T. Ben, S. Qiu, *Chem. Rev.* **2017**, *117*, 1515.

[9] a) Q. Sun, B. Aguila, J. Perman, L. D. Earl, C. Abney, Y. Cheng, H. Wei, N. Nguyen, L. Wojtas, S. Ma, *J. Am. Chem. Soc.* **2017**, *139*, 2786; b) N. Huang, L. Zhai, H. Xu, D. Jiang, *J. Am. Chem. Soc.* **2017**, *139*, 2428; c) Q. Fang, J. Wang, S. Gu, R. B. Kaspar, Z. Zhuang, J. Zheng, H. Guo, S. Qiu, Y. Yan, *J. Am. Chem. Soc.* **2015**, *137*, 8352; d) Y. Peng, Y. Huang, Y. Zhu, B. Chen, L. Wang, Z. Lai, Z. Zhang, M. Zhao, C. Tan, N. Yang, F. Shao, Y. Han, H. Zhang, *J. Am. Chem. Soc.* **2017**, *139*, 8698; e) V. S. Vyas, M. Vishwakarma, I. Moudrakovski, F. Haase, G. Savasci, C. Ochsenfeld, J. P. Spatz, B. V. Lotsch, *Adv. Mater.* **2016**, *28*, 8749; f) S. Wang, Q. Wang, P. Shao, Y. Han, X. Gao, L. Ma, S. Yuan, X. Ma, J. Zhou, X. Feng, B. Wang, *J. Am. Chem. Soc.* **2017**, *139*, 4258; g) S. Mitra, H. S. Sasmal, T. Kundu, S. Kandambeth, K. Illath, D. D. Díaz, R. Banerjee, *J. Am. Chem. Soc.* **2017**, *139*, 4513; h) Y. Lin, X. Jiang, S. T. Kim, S. B. Alahakoon, X. Hou, Z. Zhang, C. M. Thompson, R. A. Smaldone, C. Ke, *J. Am. Chem. Soc.* **2017**, *139*, 7172.

[10] a) Y. Du, H. Yang, J. M. Whiteley, S. Wan, Y. Jin, S.-H. Lee, W. Zhang, *Angew. Chem., Int. Ed.* **2016**, *55*, 1737; b) Y. Zeng, R. Zou, Y. Zhao, *Adv. Mater.* **2016**, *28*, 2855; c) L. A. Baldwin, J. W. Crowe, D. A. Pyles, P. L. McGrier, *J. Am. Chem. Soc.* **2016**, *138*, 15134; d) Y. Pramudya, J. L. Mendoza-Cortes, *J. Am. Chem. Soc.* **2016**, *138*, 15204.

[11] a) S. Lin, C. S. Diercks, Y.-B. Zhang, N. Kornienko, E. M. Nichols, Y. Zhao, A. R. Paris, D. Kim, P. Yang, O. M. Yaghi, C. J. Chang, *Science* **2015**, *349*, 1208; b) H. Xu, J. Gao, D. Jiang, *Nat. Chem.* **2015**, *7*, 905; c) S.-Y. Ding, J. Gao, Q. Wang, Y. Zhang, W.-G. Song, C.-Y. Su, W. Wang, *J. Am. Chem. Soc.* **2011**, *133*, 19816; d) Q. Sun, B. Aguila, J. A. Perman, N. Nguyen, S. Ma, *J. Am. Chem. Soc.* **2016**, *138*, 15790; e) X. Wang, X. Han, J. Zhang, X. Wu, Y. Liu, Y. Cui, *J. Am. Chem. Soc.* **2016**, *138*, 12332.

[12] a) G. H. V. Bertrand, V. K. Michaelis, T.-C. Ong, R. G. Griffin, M. Dincă, *Proc. Natl. Acad. Sci. USA* **2013**, *110*, 4923; b) M. Calik, F. Auras, L. M. Salonen, K. Bader, I. Grill, M. Handloser, D. D. Medina, M. Dogru, F. Löbermann, D. Trauner, A. Hartschuh, T. Bein, *J. Am. Chem. Soc.* **2014**, *136*, 17802.

[13] a) M.-L. Feng, D. Sarma, X.-H. Qi, K.-Z. Du, X.-Y. Huang, M. G. Kanatzidis, *J. Am. Chem. Soc.* **2016**, *138*, 12578; b) Y. Li, L. Wang, B. Li, M. Zhang, R. Wen, X. Guo, X. Li, J. Zhang, S. Li, *ACS Appl. Mater. Interfaces* **2016**, *8*, 28853; c) S. O. Odoh, G. D. Bondarevsky, J. Karpus, Q. Cui, C. He, R. Spezia, L. Gagliardi, *J. Am. Chem. Soc.* **2014**, *136*, 17484.

[14] a) C. W. Abney, S. Liu, W. Lin, *J. Phys. Chem. A* **2013**, *117*, 11558; b) C. W. Abney, R. T. Mayes, M. Piechowicz, Z. Lin, V. S. Bryantsev, G. M. Veith, S. Dai, W. Lin, *Energy Environ. Sci.* **2016**, *9*, 448.

[15] S. Kandambeth, A. Mallick, B. Lukose, M. V. Mane, T. Heine, R. Banerjee, *J. Am. Chem. Soc.* **2012**, *134*, 19524.

[16] Q. Sun, B. Aguila, S. Ma, *Mater. Chem. Front.* **2017**, *1*, 1310.

[17] S. Das, S. Brown, R. T. Mayes, C. J. Janke, C. Tsouris, L. J. Kuo, G. Gill, S. Dai, *Chem. Eng. J.* **2016**, *298*, 125.

[18] S. Vukovic, L. A. Watson, S. O. Kang, R. Custelcean, B. P. Hay, *Inorg. Chem.* **2012**, *51*, 3855.

[19] S. P. Kelley, P. S. Barber, P. H. K. Mullins, R. D. Rogers, *Chem. Commun.* **2014**, *50*, 12504.

[20] M. J. Manos, M. G. Kanatzidis, *J. Am. Chem. Soc.* **2012**, *134*, 16441.

[21] a) H. Funke, A. C. Scheinost, M. Chukalina, *Phys. Rev. B* **2005**, *71*, 094110; b) J. Timoshenko, A. Kuzmin, *Comput. Phys. Commun.* **2009**, *180*, 920; c) J. Timoshenko, A. Kuzmin, J. Purans, *Comput. Phys. Commun.* **2012**, *183*, 1237; d) J. Timoshenko, A. Kuzmin, J. Purans, *J. Phys.: Condens. Matter* **2014**, *26*, 055401; e) J. Timoshenko, K. R. Keller, A. I. Frenkel, *J. Chem. Phys.* **2017**, *146*, 114201.

[22] J. Timoshenko, A. Kuzmin, *Comput. Phys. Commun.* **2009**, *180*, 920.

[23] a) L. Zhou, M. Bosscher, C. Zhang, S. Öçubukçu, L. Zhang, W. Zhang, C. J. Li, J. Liu, M. P. Jensen, L. Lai, C. He, *Nat. Chem.* **2014**, *6*, 236; b) S. Kou, Z. Yang, F. Sun, *ACS Appl. Mater. Interfaces* **2017**, *9*, 2035.